Mon. Not. R. Astron. Soc. **273**, 157–168 (1995)

A faint galaxy redshift survey to $B = 24$

Karl Glazebrook,[1]★ Richard Ellis,[2] Matthew Colless,[3] Tom Broadhurst,[4]
Jeremy Allington-Smith[1] and Nial Tanvir[2]

[1] *Department of Physics, University of Durham, Science Laboratories, South Road, Durham DH1 3LE*
[2] *Institute of Astronomy, Madingley Road, Cambridge CB3 0HA*
[3] *Mt. Stromlo and Siding Spring Observatories, Australian National University, Weston Creek, ACT 2611, Australia*
[4] *Department of Physics and Astronomy, The John Hopkins University, Baltimore, MD 21218, USA*

Accepted 1994 October 6. Received 1994 September 12; in original form 1993 September 27

ABSTRACT

Using the multislit LDSS-2 spectrograph on the William Herschel Telescope, we have completed a redshift survey in the magnitude range $22.5 < B < 24$ which has produced 73 redshifts, representing a 73 per cent complete sample uniformly selected from four deep fields at high Galactic latitude. The survey extends out to $z > 1$ and includes the highest redshift galaxy ($z = 1.108$) yet discovered in a field sample. The median redshift, $z_{\rm MED} = 0.46$, and form of the redshift distribution constitute compelling evidence against simple luminosity evolution as an explanation of the large excess of faint galaxies [$\simeq (2–4) \times$ no-evolution] seen in this magnitude range. Rather, we identify the excess population as blue objects with $z \sim 0.4$ and B luminosities similar to local L^* galaxies, indicating a dramatic decrease in the density of such objects over the last Hubble time, and confirming the trends found in brighter redshift surveys. We also find a marked absence of *very* low-redshift galaxies ($z < 0.1$) at faint limits, severely constraining any significant steepening of the local field galaxy luminosity function at low luminosities.

Key words: surveys – galaxies: distances and redshifts – galaxies: evolution – galaxies: luminosity function, mass function – quasars: general.

1 INTRODUCTION

The number–magnitude and number–redshift distributions of faint ($B > 20$) galaxies are important probes of the geometry and evolution of the Universe. It is now well established that the number counts increasingly exceed the prediction for a non-evolving galaxy population fainter than $B \sim 20$ (Tyson 1988; Jones et al. 1991; Lilly, Cowie & Gardner 1991; Metcalfe et al. 1991). One possible explanation for this excess is that the star formation rate in galaxies was higher in the past, and that consequently galaxies were more luminous. Since they would be seen to higher redshifts than predicted from a 'no-evolution' model, a greater projected space density would result. A more radical possibility is that the comoving space density of visible galaxies has not been conserved, either because a dwarf population visible at earlier epochs has now faded beyond detection (Cowie 1991; Cowie, Songaila & Hu 1991; Babul & Rees 1992), or because present-day galaxies have been formed through self-similar merging of more numerous fragments (Rocca-Volmerange & Guiderdoni 1990; Broadhurst, Ellis & Glazebrook 1992, hereafter BEG).

To match the high surface density of galaxies found at faint magnitudes, luminosity evolution models inevitably predict a high mean redshift for the galaxies, with a substantial fraction beyond $z \simeq 1$ at $B = 24$. However, redshift surveys of several hundred galaxies to $B = 22.5$ (Broadhurst, Ellis & Shanks 1988; Colless et al. 1990, 1993) appear to show a *deficit* of high-redshift galaxies compared to the predictions of such models. Recently, some fields have been surveyed to very high completeness limits, eliminating the possibility that a significant fraction of unidentified sources lie beyond $z \simeq 1$ (Colless et al. 1993). Simple luminosity evolution models also predict that the very blue galaxies that are found in significant numbers and are fainter than $B \approx 22$ should almost all be at redshifts $z > 1$ (cf. Koo & Kron 1992), whereas the Colless et al. study of a small sample of 'flat-spectrum' galaxies found that all had $z < 1$.

These surveys constrain *luminosity* evolution at the bright end of the luminosity function, and point to some form of evolution of *number density*. As such, the interpretation

★Present address: Institute of Astronomy, Madingley Road, Cambridge CB3 0HA.

remains controversial. Metcalfe et al. (1991) and Koo & Kron (1992) have argued that, to $B=22.5$, it is still possible to reconcile the observed redshift distributions with density-conserving, mild luminosity evolution models, especially if the bright counts for $B<19$ (Heydon-Dumbleton, Collins & MacGillivray 1989; Maddox et al. 1990) are neglected and a high-density normalization for the no-evolution model is used.

More recently, Koo, Gronwall & Bruzual (1993) have introduced a no-evolution model empirically 'tuned' to fit the faint counts and redshift distributions by invoking a steep local luminosity function for dwarf blue galaxies. This model has been proposed before, and the various flavours of it are discussed extensively by Broadhurst et al. (1988).

Since the divergence between the various types of model rapidly increases at fainter apparent magnitudes, a critical test is the redshift distribution of a large sample of galaxies at a yet fainter limit. The only published work fainter than $B=22.5$ is that of Cowie et al. (1991), who measured the redshift of 12 galaxies in this range – here we report the results of a much larger redshift survey to $B=24$ carried out using the new LDSS-2 multislit spectrograph on the William Herschel Telescope at La Palma. Section 2 describes the selection of the sample and the spectroscopic observations. The results of the survey are given in Section 3, and discussed in terms of their implications for models of galaxy evolution in Section 4. Our conclusions are summarized in Section 5.

2 OBSERVATIONS

2.1 Photometric observations

The galaxies were selected from deep B and R CCD images of four equatorial fields. The details of the observations, including coordinates and field areas, are listed in Table 1. The images were obtained using the TAURUS $f/4$ focal reducer and the EEV large-format CCD on the William Herschel Telescope in 1991 May, and on the Isaac Newton Telescope using the RCA CCD in 1989 September.

Standard debiasing and sky flat-fielding reductions were applied. The TAURUS focal reducer suffers from a radial astrometric distortion of up to 3 arcsec across the field (Smail 1993), which was corrected for each individual frame by resampling the data to a linear grid before co-addition. In each frame, 20–30 objects were selected for which astrometric positions were known from wide-field AAT prime-focus plates. Using these coordinates, a 2D spline was fitted to the distortion pattern, leaving residuals <0.2 arcsec. The frames were then resampled, removing the non-linear term.

Table 1. Photometric observations.

Field	R.A. (1950)	Dec.	Area†	Time	Seeing	B_{lim}	N*
03Z3	03 39 35	−00 08 00	66.9	5000s	1.6	24.1	504
10Z2	10 44 01	+00 05 26	45.1	5000s	2.1	24.5	110
13Z2	13 41 43	+00 06 55	51.4	4200s	1.6	24.5	170
22Z3	22 02 26	−18 49 50	46.4	5000s	1.5	24.1	218

*For $22.5<B<24$.
†In arcmin^2.

Because the distortion is small compared to the size of the field, the photometric correction arising from this procedure is small ($\Delta m \approx 0.01$ mag). Its main importance is in the need for precise astrometry of target objects for the LDSS-2 multislit masks.

Objects were found automatically by first smoothing the frames with a Gaussian of width equal to the seeing, and running the FOCUS software with an area threshold equal to the seeing disc and a flux threshold 3σ ($\equiv 26.7$ mag arcsec^{-2}) above the background. Aperture photometry was performed in a 4-arcsec diameter aperture; to allow for the seeing, an aperture correction of ~ -0.3 mag (the exact value was determined independently in each field from bright stars) was applied. Obviously, for extended objects there will be a further correction; this is explored further in Section 4.

As some of the data were taken in non-photometric conditions, they were calibrated with reference to the brighter CCD data of Glazebrook et al. (1994). Our initial estimates, based on the faint isophotes used for image detection, were that the detections should be complete to $B>24$ – comparison with the published data (Metcalfe et al. 1991) shows our mean counts to be in excellent agreement to $B=24$, where the random photometric errors are ~ 0.1 mag. For $22.5<B<24$ we count 17 200 galaxies deg^{-2}, with a field–field rms variation of 40 per cent. This variation is slightly higher than expected – following the method of Glazebrook et al. (1994), we estimate from galaxy clustering that independent areas of size 50 arcmin^2 should have 25 per cent rms fluctuations. However, with only four small fields, we do not attribute any significance to this discrepancy.

In selecting the spectroscopic sample a bright cut was made at $B=22.5$, so that the entire sample would lie beyond the faint limit of the earlier LDSS-1 surveys (Colless et al. 1990, 1993). This resulted in a B-selected catalogue over the four fields of 1002 objects in the range $22.5<B<24$. As in the LDSS-1 surveys, *the object selection was based purely on apparent magnitude* – no star–galaxy separation was attempted. Since we expect a priori relatively few stars at these faint magnitudes, this will hardly affect the efficiency in measuring galaxy redshifts, but it guards against exclusion of compact extragalactic sources. Our results also allow us to measure the number of high-redshift QSOs at these magnitudes. The completeness limits and numbers of objects in the individual fields within the selected magnitude range ($22.5<B<24$) are given in Table 1.

2.2 Spectroscopic observations

The LDSS-2 faint-object spectrograph is very similar to the LDSS-1 instrument described by Wynne & Worswick (1988) and Colless et al. (1990). A full description is given by Allington-Smith et al. (1994). Briefly, LDSS-2 can accept multislit masks, with slits positioned anywhere over a field of diameter 11.5 arcmin. A choice of dispersions is available, and there is an imaging mode, primarily for the purposes of field acquisition. The main improvements over LDSS-1 are automation of all functions, better optics with an improved point-spread function, and more filter and grism options.

For the observations reported here, seven masks were used: three in the 10^h field, two in the 13^h field, and one in each of the other fields. Each mask had slits cut for between 20 and 34 objects. The slits are of length 15–20 arcsec, and arranged so that the dispersed images do not overlap in either the spectral or spatial directions.

LDSS-2 was commissioned in 1992 March–April, and during that period three masks were observed as part of the science verification. Two more masks were observed during a second run in 1992 August–September, and one of the first three was re-observed in 1993 March. A further set of masks were observed in 1994 April to extend the sample, with objects chosen in areas of forthcoming *Hubble Space Telescope* observations. A brighter lower limit ($B>20$) was used for these masks. For the rest of this paper we refer only to the $22.5<B<24$ subsample with these masks, although all of the identifications are given later in Table 3.

For all three runs a dispersion of 5.3 Å per pixel was used, with the grating blazed at 5000 Å. The detector was a Tektronix 1024 × 1024 CCD with a peak quantum efficiency of 85 per cent in the red, dropping to 40 per cent at 4000 Å. The peak measured throughput of LDSS-2 including this CCD is ≃22 per cent at 6000 Å, which, combined with the chip's readout noise of 4 e^-, meant that exposures had to be at least 1800 s long in order to be sky-limited. The spectroscopic observations are summarized in Table 2. Both the throughput and spectral resolution are a considerable improvement over that of LDSS-1 used in the earlier AAT surveys. The atmospheric seeing was also generally better than that during the AAT runs. Together with the improved optics, these factors have made it relatively straightforward to push the limiting magnitude from $B=22.5$ to $B=24$.

The individual 1800-s observations were combined with a cosmic ray filter to give final summed images. The spectra were optimally extracted according to the seeing in individual frames and calibrated using the LEXT software described in Colless et al. (1990). Both the 1D and 2D spectral information was used in confirming the reality of emission lines. Each of the spectral identifications were confirmed via independent examinations by four of the authors (KGB, RSE, MMC and TJB).

3 RESULTS

3.1 The redshift survey

In our $22.5<B<24$ sample we have observed a total of 157 objects, and identified 84 galaxies (with redshifts $0.081 \le z \le 1.108$), eight stars and two QSOs. Additionally, brighter than $B=22.5$, we have found 11 new galaxy redshifts.

For each object in the survey, Table 3 lists the mask, slit number, unique object ID number, sky coordinates, optical magnitudes and, where obtained, the redshift and rest-frame equivalent width (or upper limit thereof) of [O II] 3727 Å. Also given is a 'quality' criterion, similar to that originally defined by Colless et al. (1990). $Q=1$ indicates a reliable identification based on more than one feature; $Q=2$ indicates a less reliable identification based on a single feature (usually [O II]3727 Å or Ca H+K); $Q=3$ indicates those spectra for which no identification was possible, and $Q=4$ those for which no spectrum at all was detected. A spectral type of 'E', 'A', or 'EA' is given, depending on whether emission or absorption features or both are seen. If the object is a suspected QSO, the type is given as 'Q'. Stars are given as 'S'. The comments column lists the features found in each spectrum.

To check whether the $Q=4$ objects were genuine, and not artefacts in our original CCD data, we obtained a repeat image of the 13^h field in 1994 April. All the objects for which we attempted to obtain redshifts, including the $Q=4$ objects, were seen again. All the $Q=4$ objects lie close to the magnitude limit of the survey, so we conclude that the spectra were not detected because they are just the extreme examples of $Q=3$ objects with weak continua. Thus we include these objects in our calculations of the incompleteness, which is indeed the conservative assumption. We note that leaving them out would raise the overall completeness to ≃80 per cent and strengthen further the conclusions presented later.

3.2 Completeness and reliability of spectroscopic identifications

It can be seen from Table 2 that four of the masks are ≳70 per cent complete to $B=24$, while the remaining three are less complete. This is primarily because the latter masks were observed in rather poorer conditions of seeing and/or transparency, leading to inadequate S/N ratios for faint objects. To allow for this, we estimate from the data the limiting magnitude $B_{70\%}$ at which the completeness is ≳70 per cent. We then take this as the appropriate magnitude limit for these two fields – it is given in Table 2. We note that fainter than $B_{70\%}$ the identified and unidentified objects have the same $B-R$ colour distribution.

Table 2. Spectroscopic observations.

Mask	R.A. (1950)	Dec.	Slits	Time	Seeing	IDs	$B_{70\%}$	Slits‡	IDs‡	A_{eff}¶
03Z3_A	03 39 36.0	−00 09 05	30	14400s	1.1″	21	24.0	30	21	5.68
10Z2_A	10 43 58.0	+00 05 40	20	13500s	1.1″	15	24.0	20	15	3.90
(10Z2_B)*	10 43 58.0	+00 05 40	20	15000s	3.0″	10	23.5	11	8	4.06
10Z2_B	10 43 58.0	+00 05 40	20	10250s	1.2″	16	24.0	20	16	3.40
10HST1	10 43 58.0	+00 05 40	10†	18000s	1.5–2.0″	7	24.0	10	7	1.79
13Z2_A	13 41 42.1	+00 07 11	24	9000s	1.2″	12	23.3	13	9	7.69
13HST1	13 41 42.1	+00 07 11	19†	19800s	1.3–2.5″	10	23.5	12	9	4.50
22Z3_A	22 02 27.5	−18 49 50	34	19800s	1.3″	13	23.0	6	4	6.69

*Earlier observation.
† + extra objects with $B<22.5$ – see Table 4 for details.
‡$B<B_{70\%}$ sample.
¶Effective area in arcmin^2.

Table 3. The redshift catalogue.

Mask	Slit	ID	R.A. (1950)	Dec.	B	R	z	Ty	W_λ(Å)	Q	Comments
03z3_A	1	03.505	03 39 39.34	−00 13 43.31	23.26 ± 0.07	21.38 ± 0.02	0.617	EA	17 ± 2	1	1 OII,H+K
03z3_A	2	03.524	03 39 37.88	−00 13 21.73	23.34 ± 0.08	22.23 ± 0.04	0.616	EA	33 ± 4	1	1 OII,H+K,Balmer,G,Hβ+?
03z3_A	3	03.944	03 39 34.05	−00 13 07.06	22.86 ± 0.06	No Data	0.303	A	≤ 4	1	1 H+K,Mgb
03z3_A	4	03.572	03 39 38.46	−00 12 39.43	23.81 ± 0.13	23.30 ± 0.12	UnID	—	—	4	4 Missing?
03z3_A	5	03.595	03 39 40.90	−00 12 19.18	22.68 ± 0.04	21.15 ± 0.02	0.594	EA	10 ± 2	1	1 OII,H+K,Hδ-,MgII-
03z3_A	6	03.608	03 39 41.49	−00 12 04.53	23.87 ± 0.12	23.40 ± 0.12	0.893	E	63 ± 12	2	2 ?OII
03z3_A	7	03.619	03 39 36.03	−00 11 50.49	23.18 ± 0.07	22.38 ± 0.05	0.750	E	41 ± 3	2	2 ?OII
03z3_A	8	03.644	03 39 38.76	−00 11 27.05	23.94 ± 0.13	21.96 ± 0.03	0.000	S	—	1	1 M star
03z3_A	9	03.668	03 39 40.47	−00 11 09.96	23.19 ± 0.07	22.27 ± 0.04	0.432	E	84 ± 3	1	1 OII,?Hγ+,Hβ+,OIII,OIII
03z3_A	10	03.687	03 39 39.49	−00 10 50.83	22.83 ± 0.05	21.38 ± 0.02	0.302	EA	18 ± 2	1	1 OII,H+K,Hδ-,?G,?Hβ+,Mgb
03z3_A	11	03.723	03 39 35.93	−00 10 21.58	22.51 ± 0.04	21.58 ± 0.02	0.315	EA	54 ± 5	1	1 OII,H+K,Hβ+,OIII,OIII
03z3_A	12	03.740	03 39 38.47	−00 10 06.59	23.67 ± 0.10	22.75 ± 0.07	0.432	E	54 ± 7	1	1 OII,OIII,OIII
03z3_A	13	03.763	03 39 42.52	−00 09 41.84	23.90 ± 0.12	22.49 ± 0.05	UnID	—	—	4	4 Missing?
03z3_A	14	03.773	03 39 43.78	−00 09 27.67	22.87 ± 0.05	21.96 ± 0.03	0.375	EA	62 ± 6	1	1 OII,?Hβ+,?OIII,OIII
03z3_A	15	03.788	03 39 42.75	−00 09 11.49	23.91 ± 0.13	22.93 ± 0.08	0.540	E	34 ± 5	2	2 OII,OIII, break
03z3_A	16	03.803	03 39 41.62	−00 08 58.35	23.77 ± 0.12	23.63 ± 0.16	UnID	—	—	3	3 Weak
03z3_A	17	03.820	03 39 43.79	−00 08 39.03	23.86 ± 0.13	23.07 ± 0.10	0.487	E	31 ± 4	2	2 ?OII
03z3_A	18	03.842	03 39 39.25	−00 08 14.04	23.60 ± 0.11	Too faint	0.000	S	—	1	1 Star
03z3_A	19	03.023	03 39 32.71	−00 07 46.31	23.97 ± 0.13	23.03 ± 0.10	UnID	—	—	3	3 Weak
03z3_A	20	03.033	03 39 26.51	−00 07 32.81	23.99 ± 0.12	22.65 ± 0.07	0.646	E	69 ± 5	2	2 ?OII
03z3_A	21	03.059	03 39 30.40	−00 07 19.60	23.22 ± 0.06	22.15 ± 0.05	0.596	E	60 ± 2	2	2 ?OII,?Hδ+-
03z3_A	22	03.096	03 39 26.01	−00 06 42.00	23.85 ± 0.10	23.11 ± 0.10	0.581	E	85 ± 3	2	2 ?OII
03z3_A	23	03.114	03 39 28.94	−00 06 26.18	23.32 ± 0.06	22.89 ± 0.08	UnID	—	—	3	3 Featureless
03z3_A	24	03.132	03 39 29.58	−00 06 07.44	23.91 ± 0.11	22.75 ± 0.07	0.288	EA	37 ± 4	1	1 OII,OIII
03z3_A	25	03.155	03 39 31.40	−00 05 47.00	23.60 ± 0.08	No Data	UnID	—	—	4	4 Missing?
03z3_A	26	03.202	03 39 29.23	−00 05 19.89	23.51 ± 0.07	21.87 ± 0.03	0.746	E	12 ± 2	2	2 ?OII,??H+K (?OII=MgII at z=1.324?)
03z3_A	27	03.219	03 39 30.42	−00 05 05.51	23.59 ± 0.08	22.48 ± 0.06	0.601	E	37 ± 4	2	2 ?OII
03z3_A	28	03.241	03 39 31.36	−00 04 48.28	23.68 ± 0.08	23.03 ± 0.09	UnID	—	—	3	3 Weak
03z3_A	29	03.279	03 39 31.46	−00 04 20.76	23.97 ± 0.12	23.79 ± 0.18	UnID	—	—	4	4 Missing?
03z3_A	30	03.307	03 39 31.40	−00 04 05.83	23.28 ± 0.07	22.29 ± 0.05	UnID	—	—	3	3 Featureless
10z2_A	1	10.205	10 43 58.32	00 01 47.32	23.52 ± 0.09	23.50 ± 0.21	UnID	—	—	3	3 Featureless
10z2_A	2	10.227	10 43 53.70	00 02 27.39	23.98 ± 0.11	23.55 ± 0.19	UnID	—	—	3	3 Weak
10z2_A	3	10.233	10 43 51.83	00 02 40.73	22.72 ± 0.04	20.99 ± 0.02	0.307	EA	20 ± 2	1	1 OII,H+K,Hδ-,Hγ-,?OIII
10z2_A	4	10.262	10 43 52.62	00 03 25.60	23.77 ± 0.10	21.70 ± 0.03	0.294	EA	12 ± 4	1	1 OII,FeI,H+K,?OIII
10z2_A	5	10.250	10 44 06.38	00 03 04.36	23.56 ± 0.08	22.99 ± 0.12	UnID	—	—	3	3 Featureless
10z2_A	6	10.279	10 44 00.14	00 03 47.02	22.54 ± 0.03	22.27 ± 0.06	0.634	E	55 ± 1	1	1 OII,Hβ+,OIII,OIII
10z2_A	7	10.288	10 43 59.13	00 04 07.80	23.37 ± 0.07	23.08 ± 0.12	1.108	EA	65 ± 10	1	1 OII,MgI-,MgII-,?FeII-
10z2_A	8	10.313	10 44 06.18	00 04 55.71	23.88 ± 0.11	21.20 ± 0.02	0.000	S	—	1	1 M star
10z2_A	9	10.328	10 44 05.38	00 05 29.63	23.16 ± 0.06	21.25 ± 0.02	0.207	A	19 ± 6	1	1 H+K,G,Mgb,NaD
10z2_A	10	10.022	10 44 01.49	00 05 48.04	23.96 ± 0.15	Too faint	0.924	E	17 ± 8	2	2 ?OII,?MgII-
10z2_A	11	10.031	10 43 52.15	00 06 04.33	23.52 ± 0.10	22.45 ± 0.07	0.278	E	41 ± 4	1	1 OII,Hβ+,OIII,OIII
10z2_A	12	10.048	10 44 10.82	00 06 34.51	22.93 ± 0.06	20.78 ± 0.02	0.276	EA	27 ± 2	1	1 OII,H+K,Hβ+,OIII,OIII
10z2_A	13	10.066	10 44 04.19	00 07 00.49	23.30 ± 0.08	21.80 ± 0.05	0.368	EA	15 ± 2	1	1 OII,H+K,Hβ+,OIII,Mgb
10z2_A	14	10.080	10 44 03.35	00 07 38.20	22.78 ± 0.05	21.93 ± 0.05	0.621	E	37 ± 1	1	1 OII,?Hδ-,?Hβ+,OIII
10z2_A	15	10.088	10 43 56.16	00 07 56.80	22.70 ± 0.04	21.60 ± 0.04	0.177	EA	≤ 8	1	1 H+K,G,Hα+
10z2_A	16	10.073	10 43 51.93	00 07 16.95	23.83 ± 0.12	Too faint	UnID	—	—	4	4 Missing?
10z2_A	17	10.109	10 43 59.45	00 08 39.33	23.66 ± 0.11	20.74 ± 0.02	0.492	A	—	1	1 ?OII,H+K,Hδ-,G,Hγ-
10z2_A	18	10.120	10 43 55.03	00 08 57.26	23.51 ± 0.09	21.11 ± 0.02	0.579	EA	6 ± 1	1	1 ?OII,H+K,FeI,G (OII on NS)
10z2_A	19	10.131	10 44 11.93	00 09 20.17	23.37 ± 0.12	22.75 ± 0.09	UnID	—	—	4	4 Missing?
10z2_A	20	10.301	10 44 02.95	00 04 36.28	23.51 ± 0.08	21.97 ± 0.04	0.323	EA	25 ± 5	1	1 OII,OIII,OIII
10z2_B	1	10.206	10 44 02.71	00 01 48.30	23.48 ± 0.08	22.69 ± 0.09	1.599	Q	—	1	1 QSO? - MgII,CIII],CIV
10z2_B	2	10.223	10 43 55.52	00 02 23.66	23.99 ± 0.12	23.61 ± 0.19	0.296	E	58 ± 8	1	1 OII,Hβ,OII, ?H+K
10z2_B	3	10.236	10 44 05.91	00 02 43.60	23.81 ± 0.10	Too faint	UnID	—	—	4	4 Missing?
10z2_B	4	10.248	10 44 00.02	00 03 00.54	23.23 ± 0.06	21.07 ± 0.02	0.314	A	≤ 3	1	1 H+K
10z2_B	5	10.260	10 43 56.37	00 03 20.87	23.49 ± 0.08	21.95 ± 0.05	0.563	EA	17 ± 2	1	1 OII,H+K,Balmer
10z2_B	6	10.277	10 44 11.03	00 03 44.77	23.10 ± 0.05	22.34 ± 0.06	UnID	—	—	3	3 Incorrect mag?
10z2_B	7	10.286	10 44 02.43	00 04 03.01	22.65 ± 0.04	21.43 ± 0.03	0.559	EA	33 ± 2	1	1 OII,H+K,Balmer
10z2_B	8	10.300	10 44 00.65	00 04 36.37	23.96 ± 0.12	21.21 ± 0.02	0.000	S	—	1	1 M star (flux too low for mag)
10z2_B	9	10.315	10 44 02.62	00 05 00.55	23.98 ± 0.12	Too faint	UnID	—	—	3	3 Weak
10z2_B	10	10.330	10 44 03.23	00 05 31.41	23.70 ± 0.09	22.26 ± 0.06	0.324	E	50 ± 3	1	1 OII,Hβ,OIII,?H+K
10z2_B	11	10.025	10 43 59.13	00 05 55.72	22.68 ± 0.04	23.62 ± 0.24	2.749	Q	—	1	1 Lyα,CIV,?CIII]
10z2_B	12	10.036	10 43 59.43	00 06 16.07	23.02 ± 0.06	21.51 ± 0.03	0.478	EA	30 ± 4	1	1 OII,OIII,,H+K,Balmer
10z2_B	13	10.061	10 44 01.02	00 06 52.30	23.14 ± 0.07	20.92 ± 0.02	0.384	A	≤ 3	1	1 H+K,G,Hβ,Mgb
10z2_B	14	10.047	10 43 53.94	00 06 34.04	23.87 ± 0.13	23.98 ± 0.38	0.199	E	26 ± 4	1	1 OII,Hβ,OIII,?H+K,?Balmer
10z2_B	15	10.071	10 43 56.75	00 07 10.47	22.84 ± 0.05	20.50 ± 0.01	0.476	EA	10 ± 2	1	1 OII,H+K,G,Balmer
10z2_B	16	10.077	10 43 55.39	00 07 33.06	23.70 ± 0.11	21.48 ± 0.03	0.436	A	≤ 2	1	1 H+K,G,Balmer
10z2_B	17	10.086	10 43 57.58	00 07 50.52	23.73 ± 0.12	23.93 ± 0.31	UnID	—	—	3	3 Weak
10z2_B	18	10.107	10 44 07.20	00 08 38.23	23.87 ± 0.14	22.10 ± 0.06	0.448	E	55 ± 5	1	1 OII,Hβ,OIII
10z2_B	19	10.122	10 44 02.20	00 09 00.41	23.11 ± 0.06	22.03 ± 0.06	0.724	EA	30 ± 2	2	2 OII,Hz,K,(H in sky abs?)
10z2_B	20	10.130	10 44 08.65	00 09 19.88	23.19 ± 0.07	20.87 ± 0.02	0.456	EA	8 ± 2	1	1 OII,H+K,Balmer,?OIII
10HST1	1	10.204	10 43 57.17	00 01 45.04	23.10 ± 0.06	22.61 ± 0.09	0.742	EA	42 ± 3	1	1 OII,FeII,break?
10HST1	2	10.218	10 43 57.36	00 01 57.47	20.72 ± 0.00	18.93 ± 0.00	0.097	A	≤ 5	1	1 H+K,G,Hβ-,NaD
10HST1	3	10.222	10 43 57.69	00 02 15.95	22.39 ± 0.03	22.75 ± 0.10	1.999	Q	—	1	1 QSO CIV,CIII,no La?
10HST1	4	10.227	10 43 53.70	00 02 27.39	23.98 ± 0.11	23.55 ± 0.19	UnID	—	—	3	3 Weak
10HST1	5	10.235	10 43 55.01	00 02 42.11	21.95 ± 0.02	19.65 ± 0.00	0.000	S	—	1	1 Mstar
10HST1	6	10.249	10 43 51.44	00 03 02.44	23.50 ± 0.08	22.35 ± 0.06	0.466	EA	8 ± 4	1	1 OII,OIII,H+K
10HST1	7	10.255	10 43 55.59	00 03 15.08	22.52 ± 0.03	21.44 ± 0.03	0.149	EA	42 ± 5	1	1 OII,OIII,Hα,H+K
10HST1	8	10.273	10 43 56.99	00 03 35.55	22.47 ± 0.03	19.47 ± 0.00	0.435	EA	3 ± 1	1	1 OII,H+K,G,
10HST1	9	10.315	10 44 02.62	00 05 00.55	23.98 ± 0.12	Too faint	UnID	—	—	4	4 Missing
10HST1	10	10.332	10 44 01.27	00 05 38.72	22.78 ± 0.04	20.60 ± 0.01	0.000	S	—	1	1 late-type star

Table 3 – *continued*

Mask	Slit	ID	R.A. (1950)	Dec.	B	R	z	Ty	W_λ(Å)	Q	Comments
10HST1	11	10.028	10 44 03.88	00 05 59.00	21.89 ± 0.02	20.64 ± 0.01	0.582	EA	8 ± 1	1	1 OII,OIII,Balmer,
10HST1	12	10.032	10 44 01.53	00 06 09.78	23.94 ± 0.14	Too faint	UnID	—	—	4	4 Missing
10HST1	13	10.040	10 43 57.82	00 06 21.31	23.73 ± 0.12	20.96 ± 0.02	0.476	A	≤ 7	1	1 H+K,G,Hβ-,Mgb
10HST1	14	10.051	10 44 01.99	00 06 35.95	22.84 ± 0.05	22.65 ± 0.10	0.081	E	20 ± 9	1	1 Hα,OIII
10HST1	15	10.064	10 44 04.88	00 06 54.81	22.11 ± 0.03	19.80 ± 0.00	0.000	S	—	1	1 Mstar
10HST1	16	10.086	10 43 57.58	00 07 50.52	23.73 ± 0.12	23.93 ± 0.31	0.758	E	24 ± 2	2	2 OII only
10HST1	17	10.092	10 44 01.26	00 08 09.05	22.16 ± 0.03	21.18 ± 0.03	UnID	—	—	3	3 Featureless
10HST1	18	10.105	10 43 57.66	00 08 25.41	20.02 ± 0.00	17.83 ± 0.00	0.000	S	—	1	1 Mstar
10HST1	19	10.116	10 43 55.84	00 08 50.06	21.73 ± 0.02	21.51 ± 0.04	1.256	Q	—	1	1 QSO
10HST1	20	10.126	10 43 58.72	00 09 05.44	22.30 ± 0.03	21.69 ± 0.05	0.000	S	—	1	1 early-type star
13z2_A	1	13.304	13 41 42.70	00 02 49.73	23.66 ± 0.09	23.66 ± 0.09	UnID	—	—	4	4 Missing?
13z2_A	2	13.311	13 41 41.44	00 03 05.87	23.38 ± 0.06	22.04 ± 0.02	UnID	—	—	3	3 Weak
13z2_A	3	13.323	13 41 38.73	00 03 24.07	23.16 ± 0.05	21.29 ± 0.01	0.385	EA	19 ± 2	1	1 OII,H+K,FeI,Hδ-
13z2_A	4	13.347	13 41 48.56	00 03 45.36	23.09 ± 0.05	22.32 ± 0.03	UnID	—	—	3	3 Weak
13z2_A	5	13.370	13 41 35.39	00 04 11.08	23.78 ± 0.09	22.49 ± 0.03	UnID	—	—	3	3 Weak (?em@4775,6745?)
13z2_A	6	13.384	13 41 39.08	00 04 29.73	23.65 ± 0.09	22.58 ± 0.03	UnID	—	—	3	3 Weak
13z2_A	7	13.402	13 41 45.60	00 04 49.09	23.24 ± 0.06	22.11 ± 0.02	0.830	E	44 ± 4	2	2 OII
13z2_A	8	13.420	13 41 34.97	00 05 14.33	23.85 ± 0.10	22.07 ± 0.03	UnID	—	—	3	3 Weak
13z2_A	9	13.444	13 41 39.28	00 05 38.11	23.21 ± 0.06	22.60 ± 0.04	UnID	—	—	3	3 Weak
13z2_A	10	13.465	13 41 40.75	00 05 59.44	23.23 ± 0.06	21.90 ± 0.02	0.556	EA	14 ± 3	1	1 OII,H+K,Hδ-,Hγ-
13z2_A	11	13.480	13 41 43.00	00 06 14.39	22.83 ± 0.04	21.49 ± 0.01	0.556	EA	34 ± 5	2	2 ?OII
13z2_A	12	13.504	13 41 48.79	00 06 48.80	23.40 ± 0.06	22.05 ± 0.02	UnID	—	—	3	3 Weak
13z2_A	13	13.517	13 41 40.95	00 07 06.57	23.94 ± 0.10	22.51 ± 0.03	0.462	E	36 ± 7	2	2 ?OII
13z2_A	14	13.016	13 41 45.13	00 07 28.62	22.82 ± 0.03	21.89 ± 0.01	UnID	—	—	3	3 Featureless
13z2_A	15	13.027	13 41 42.29	00 07 50.95	22.86 ± 0.03	22.48 ± 0.02	0.089	E	41 ± 7	1	1 Hβ+,OIII,OIII,Hα (?OII?,?EW?)
13z2_A	16	13.038	13 41 44.33	00 08 10.76	22.88 ± 0.03	21.40 ± 0.00	0.424	EA	12 ± 2	1	1 OII,H+K,G
13z2_A	17	13.056	13 41 38.74	00 08 38.20	22.70 ± 0.03	21.33 ± 0.00	0.556	EA	32 ± 2	2	2 ?OII
13z2_A	18	13.078	13 41 42.95	00 08 57.78	23.33 ± 0.05	21.85 ± 0.01	UnID	—	—	3	3 Weak
13z2_A	19	13.087	13 41 35.40	00 09 16.17	23.17 ± 0.04	20.71 ± 0.00	0.359	A	≤ 2	1	1 H+K,G
13z2_A	20	13.106	13 41 44.15	00 09 36.95	22.92 ± 0.03	21.66 ± 0.01	0.187	E	59 ± 14	1	1 OII,Hβ+,OIII,Hα
13z2_A	21	13.123	13 41 42.76	00 09 57.38	23.45 ± 0.05	22.11 ± 0.02	0.536	E	32 ± 3	2	2 ?OII
13z2_A	22	13.160	13 41 47.41	00 10 43.91	23.53 ± 0.06	21.96 ± 0.02	0.335	E	35 ± 4	1	1 OII,OIII
13z2_A	23	13.177	13 41 52.15	00 11 05.46	23.02 ± 0.04	22.15 ± 0.02	UnID	—	—	3	3 Weak
13z2_A	24	13.190	13 41 44.30	00 11 27.96	23.76 ± 0.07	21.40 ± 0.00	UnID	—	—	3	3 Weak
13HST1	1	13.311	13 41 41.44	00 03 05.87	23.38 ± 0.06	22.04 ± 0.02	0.458	EA	21 ± 5	2	2 OII,H+K
13HST1	2	13.325	13 41 40.71	00 03 25.88	23.40 ± 0.07	20.70 ± 0.00	0.000	S	—	1	1 Mstar
13HST1	3	13.344	13 41 38.97	00 03 41.64	23.24 ± 0.06	22.59 ± 0.04	0.452	A	≤ 117	2	2 H+K,
13HST1	4	13.358	13 41 48.83	00 03 57.17	21.99 ± 0.02	21.02 ± 0.00	UnID	—	—	3	3 Weak
13HST1	5	13.367	13 41 39.47	00 04 07.10	23.75 ± 0.10	22.60 ± 0.04	UnID	—	—	4	4 Missing
13HST1	6	13.378	13 41 47.15	00 04 21.71	22.67 ± 0.03	21.73 ± 0.02	UnID	—	—	3	3 Weak
13HST1	7	13.388	13 41 47.53	00 04 36.43	22.75 ± 0.04	20.55 ± 0.00	0.443	A	≤ 3	1	1 H+K,G
13HST1	8	13.400	13 41 45.16	00 04 49.14	21.87 ± 0.02	20.57 ± 0.00	0.830	E	19 ± 1	1	1 OII
13HST1	9	13.417	13 41 40.97	00 05 08.24	22.74 ± 0.04	20.43 ± 0.00	0.283	A	≤ 6	1	1 H+K,G,Hβ-,Mgb
13HST1	10	13.452	13 41 43.26	00 05 40.86	22.00 ± 0.02	20.72 ± 0.00	0.451	A	≤ 4	2	2 H+K,G
13HST1	11	13.460	13 41 44.21	00 05 54.13	22.61 ± 0.03	21.86 ± 0.02	UnID	—	—	3	3 Weak
13HST1	12	13.469	13 41 42.38	00 06 03.46	23.07 ± 0.05	21.25 ± 0.01	0.493	EA	13 ± 1	1	1 OII,H+K,OIII
13HST1	13	13.484	13 41 45.37	00 06 24.56	20.58 ± 0.00	18.13 ± 0.00	0.000	S	—	1	1 Mstar
13HST1	14	13.492	13 41 40.63	00 06 37.63	23.62 ± 0.08	22.29 ± 0.03	UnID	—	—	4	4 Missing
13HST1	15	13.510	13 41 43.50	00 06 55.26	23.01 ± 0.05	20.89 ± 0.00	0.566	EA	7 ± 1	1	1 OII,H+K,Hδ-,Hγ-,Hβ-
13HST1	16	13.519	13 41 41.84	00 07 06.81	22.39 ± 0.03	20.75 ± 0.00	0.278	EA	8 ± 3	1	1 OII?,H+K,Hβ-,Mgb,NaD
13HST1	17	13.012	13 41 42.71	00 07 22.33	22.09 ± 0.01	21.05 ± 0.00	UnID	—	—	3	3 Featureless
13HST1	18	13.028	13 41 44.80	00 07 52.37	23.41 ± 0.05	22.01 ± 0.01	0.426	EA	4 ± 21	2	2 OII,OIII,Balmer
13HST1	19	13.034	13 41 42.78	00 08 04.94	23.73 ± 0.07	22.69 ± 0.03	UnID	—	—	3	3 Featureless
13HST1	20	13.079	13 41 42.11	00 08 59.55	21.78 ± 0.01	19.65 ± 0.00	0.279	A	≤ 2	1	1 H+K,G,Hβ-,NaD,Mgb
13HST1	21	13.091	13 41 43.02	00 09 21.15	23.64 ± 0.06	22.46 ± 0.02	UnID	—	—	3	3 Weak
13HST1	22	13.098	13 41 43.19	00 09 32.00	23.22 ± 0.04	22.56 ± 0.03	UnID	—	—	3	3 Featureless
13HST1	23	13.116	13 41 46.87	00 09 50.09	22.79 ± 0.03	20.82 ± 0.00	0.363	EA	7 ± 2	1	1 OII,H+K,Hβ-
13HST1	24	13.131	13 41 47.17	00 10 02.93	21.70 ± 0.01	19.91 ± 0.00	0.326	EA	4 ± 1	1	1 OII,Hδ-,G,Hβ-
13HST1	25	13.139	13 41 41.42	00 10 13.89	23.73 ± 0.07	22.89 ± 0.04	0.146	E	29 ± 6	1	1 OII,OIII,Hα
13HST1	26	13.151	13 41 41.17	00 10 23.60	20.62 ± 0.00	19.86 ± 0.00	0.148	A	≤ 9	1	1 H+K,G,Hβ-
13HST1	27	13.161	13 41 46.57	00 10 39.68	20.18 ± 0.00	18.85 ± 0.00	0.088	A	≤ 3	1	1 H+K,G,Hβ-,Mgb,NaD
13HST1	28	13.164	13 41 51.34	00 10 52.48	23.86 ± 0.08	22.16 ± 0.02	UnID	—	—	3	3 Weak
13HST1	29	13.180	13 41 46.61	00 11 07.51	22.16 ± 0.02	20.14 ± 0.00	0.000	S	—	1	1 Mstar
13HST1	30	13.186	13 41 48.61	00 11 19.60	23.71 ± 0.07	22.50 ± 0.03	UnID	—	—	3	3 Weak
13HST1	31	13.191	13 41 46.84	00 11 29.32	21.93 ± 0.01	21.16 ± 0.00	0.242	EA	65 ± 4	1	1 OII,H+K,OIII,Hα
22z3_A	1	22.303	22 02 21.04	−18 54 37.33	23.92 ± 0.12	23.11 ± 0.12	UnID	—	—	4	4 Missing?
22z3_A	2	22.310	22 02 19.43	−18 54 23.82	23.47 ± 0.09	22.43 ± 0.06	UnID	—	—	3	3 Weak
22z3_A	3	22.322	22 02 22.94	−18 54 09.69	22.82 ± 0.05	Too faint	0.469	EA	8 ± 2	1	1 OII,H+K,Hδ-
22z3_A	4	22.332	22 02 25.25	−18 53 51.99	23.19 ± 0.07	Too faint	0.824	E	64 ± 3	2	2 ?OII
22z3_A	5	22.342	22 02 24.45	−18 53 19.59	22.86 ± 0.05	21.53 ± 0.03	0.263	E	65 ± 3	1	1 OII,Hβ+,OIII,OIII
22z3_A	6	22.346	22 02 29.08	−18 53 03.66	23.53 ± 0.10	22.10 ± 0.05	0.622	E	29 ± 3	2	2 ?OII
22z3_A	7	22.358	22 02 29.25	−18 52 42.81	23.09 ± 0.06	21.81 ± 0.04	UnID	—	—	3	3 Featureless
22z3_A	8	22.370	22 02 32.18	−18 52 28.59	23.33 ± 0.08	23.28 ± 0.14	UnID	—	—	3	3 Weak
22z3_A	9	22.378	22 02 32.17	−18 52 13.42	23.42 ± 0.09	22.60 ± 0.08	UnID	—	—	3	3 Weak
22z3_A	10	22.381	22 02 23.61	−18 51 58.63	23.47 ± 0.09	21.24 ± 0.02	0.000	S	—	1	1 M star
22z3_A	11	22.390	22 02 22.24	−18 51 43.21	23.85 ± 0.13	22.91 ± 0.10	UnID	—	—	3	3 Weak
22z3_A	12	22.406	22 02 29.87	−18 51 27.55	23.64 ± 0.10	23.95 ± 0.26	UnID	—	—	4	4 Missing?
22z3_A	13	22.412	22 02 27.16	−18 51 12.44	23.84 ± 0.13	22.41 ± 0.06	UnID	—	—	3	3 Weak
22z3_A	14	22.442	22 02 33.68	−18 50 34.87	22.62 ± 0.05	No Data	0.549	EA	18 ± 2	2	2 ?OII,?H+K,?FeI
22z3_A	15	22.434	22 02 27.91	−18 50 17.22	23.32 ± 0.08	22.02 ± 0.05	0.621	E	45 ± 3	2	2 ?OII
22z3_A	16	22.438	22 02 21.41	−18 50 03.81	23.41 ± 0.09	22.17 ± 0.05	0.603	EA	46 ± 4	2	2 ?OII,?H+K,?FeI

Table 3 – *continued*

Mask	Slit	ID	R.A.	(1950) Dec.	B	R	z	Ty	W_λ(Å)	Q	Comments
22z3_A	17	22.002	22 02 26.17	−18 49 50.57	22.56 ± 0.05	21.40 ± 0.02	0.399	E	31 ± 3	1	1 OII,Hβ+,OIII,OIII
22z3_A	18	22.014	22 02 19.11	−18 49 23.00	23.35 ± 0.09	No Data	UnID	—	—	3	3 Weak
22z3_A	19	22.027	22 02 27.82	−18 49 03.57	23.08 ± 0.07	22.26 ± 0.05	UnID	—	—	3	3 Weak
22z3_A	20	22.038	22 02 27.04	−18 48 51.37	23.45 ± 0.10	22.35 ± 0.05	UnID	—	—	3	3 Weak
22z3_A	21	22.052	22 02 26.40	−18 48 33.72	23.35 ± 0.09	21.30 ± 0.02	0.000	S	—	1	1 M star
22z3_A	22	22.065	22 02 24.25	−18 48 18.11	23.98 ± 0.16	23.75 ± 0.21	UnID	—	—	4	4 Missing
22z3_A	23	22.075	22 02 22.83	−18 48 02.50	23.48 ± 0.10	Too faint	UnID	—	—	3	3 Weak
22z3_A	24	22.090	22 02 24.90	−18 47 48.50	23.67 ± 0.12	22.66 ± 0.07	UnID	—	—	3	3 Featureless
22z3_A	25	22.270	22 02 24.14	−18 47 32.86	23.90 ± 0.15	Too faint	0.769	E	70 ± 7	2	2 ?OII
22z3_A	26	22.108	22 02 27.65	−18 47 18.77	23.76 ± 0.14	Too faint	UnID	—	—	4	4 Missing?
22z3_A	27	22.126	22 02 29.13	−18 47 00.30	22.73 ± 0.05	22.00 ± 0.04	UnID	—	—	3	3 Featureless
22z3_A	28	22.144	22 02 28.01	−18 46 38.02	23.96 ± 0.16	23.35 ± 0.14	UnID	—	—	4	4 Missing?
22z3_A	29	22.159	22 02 27.52	−18 46 22.02	23.56 ± 0.11	22.92 ± 0.09	UnID	—	—	3	3 Weak
22z3_A	30	22.172	22 02 26.53	−18 46 03.62	23.80 ± 0.14	23.20 ± 0.12	1.067	E	69 ± 15	2	2 OII, ?MgI, ?MgII
22z3_A	31	22.181	22 02 31.39	−18 45 52.36	23.96 ± 0.17	23.61 ± 0.19	UnID	—	—	4	4 Missing?
22z3_A	32	22.190	22 02 26.23	−18 45 19.02	23.87 ± 0.14	22.99 ± 0.09	UnID	—	—	3	3 Weak
22z3_A	33	22.205	22 02 25.81	−18 44 58.86	23.89 ± 0.14	22.34 ± 0.05	0.300	E	21 ± 6	1	1 OII,Hβ+,OIII,OIII
22z3_A	34	22.216	22 02 22.45	−18 44 43.40	22.86 ± 0.06	22.48 ± 0.06	UnID	—	—	3	3 Weak

In our final $B < B_{70\%}$ sample there are 111 objects in total, 81 of which have identifications, so the overall completeness is 73 per cent. Of these, 73 are galaxies, six are faint stars, and two we identify as QSOs owing to their high redshift and broad lines. For our later analysis we also consider a smaller, but more complete, subsample: if we use only the four best masks (03z3–A and the 10^h masks) and take a uniform magnitude cut of $22.5 < B \leq 23.5$, then we have an 89 per cent complete subsample (30 galaxies, two QSOs, one star and four unidentified objects). We examine these samples in Section 4.

62 objects have $Q=1$, and 19 have $Q=2$. The mask 10z2–B was observed twice, the second time in much better conditions with a much greater limiting depth. This gives us a valuable internal check on the reliability of our quality values. The second observation was reduced a year after the first, with no reference to the earlier notes until after the identifications were established. The results of this exercise are illuminating – all four of the original $Q=1$ identifications and four out of six of the $Q=2$ identifications on the earlier observation were correct. All the [O II] equivalent widths were the same within the errors. This gives us confidence in the overall reliability of our identifications.

As it is impractical to show all 81 spectra here, we have chosen 11 of them, using a random number generator, to demonstrate the typical quality of the spectra and the reliability of the identifications. The spectra (shown in Fig. 1) are optimally smoothed with a 15-Å FWHM Gaussian to match the instrumental response. The sky-subtraction is occasionally poor near the bright sky lines at 5577, 5892 and 6300 Å, so these parts of the spectra, together with the odd residual cosmic ray, have been blanked out in the figure. Our line identifications are marked. It should be re-emphasized that our identifications do not rest solely on the 1D spectra – the 2D sky-subtracted images were also scrutinized to distinguish bright emission lines from cosmic rays.

The remaining twelfth object in Fig. 1 (top left, 10.288) is not randomly chosen – we show it because it is the highest redshift galaxy yet seen in a published field sample ($z=1.108$). It shows strong extended [O II] emission and, interestingly, several absorption features which are clearly identified with Mg II, Mg I and Fe II. It is a much more secure identification than the $z=1.018$ object of Thompson & Djorgovski (1991), whose spectrum only revealed [O II] and was, in any case, close to a QSO. The Mg II/Mg I equivalent width ratio is typical of those seen in the stronger Mg absorption-line systems (Steidel & Sargent 1992), and the $B-R=0.3$ colour indicates that this is a flat-spectrum object. Neither its luminosity, $M_B \simeq -18.8 \simeq 0.4L^*$ assuming flat-spectrum ($\Delta f_\nu = 0$) K-corrections, nor its redshift is particularly unusual. As we will show in Section 4, the object simply represents the high-redshift tail of the distribution of our deep data, even without any evolution in luminosity.

4 DISCUSSION

The magnitude–redshift relation for all the identified galaxies is shown in Fig. 2, where we have also plotted previously published B-selected field samples (Peterson et al. 1986; Broadhurst et al. 1988; Colless et al. 1990; Cowie et al. 1991; Ellis & Broadhurst 1993, in preparation). The deepest previous data are provided by Cowie et al. (1991), who measured 12 redshifts forming a complete sample in the range $22.5 \leq B \leq 24$ acquired via single-slit spectroscopy with an average integration time of 15 000 s per object. Other deep surveys have been published recently, but these involve selection in bands other than B. Colless et al. (1993) obtained 11 redshifts for a sample of flat-spectrum galaxies with $22 < R < 23$ with LDSS-1, and Lilly (1993) and Tresse et al. (1993) have various I-limited surveys underway. Concentrating on the B-limited samples, the figure shows a smooth trend, both in terms of the upper redshift envelope and the mean redshift increasing slowly for progressively fainter limits.

4.1 Faint QSO number densities

Before discussing the detailed properties of the galaxy population, we consider the number of QSOs found. The observed fraction of QSOs corresponds to a number density of 266^{+572}_{-213} deg^{-2} mag^{-1} (95 per cent confidence limits calculated using Poisson statistics, as in Gehrels 1986) at $B \simeq 23.2$ (mean magnitude of sample). The lower limit is, of course, more secure than the upper limit due to the number of unidentified objects in the sample, although QSOs with their

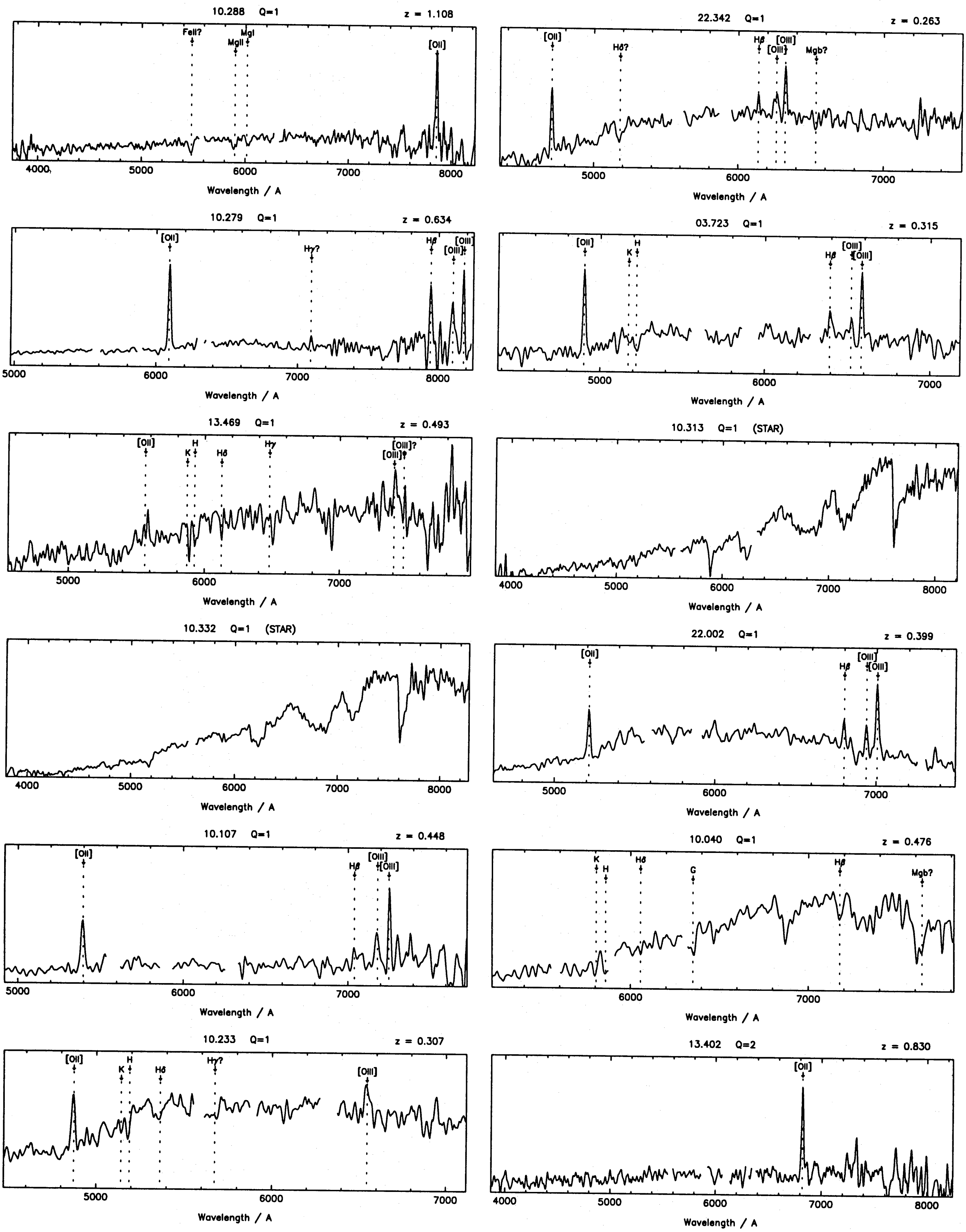

Figure 1. Randomly selected spectra (except for object 10.288) from the LDSS-2 redshift survey, showing the claimed features by which they were identified. Gaps in the spectra represent regions where poorly subtracted night-sky lines, or occasional CCD defects and residual cosmic rays, have been removed. The spectra have been approximately relatively flux-calibrated (in f_λ) by dividing by the telescope + instrument throughput.

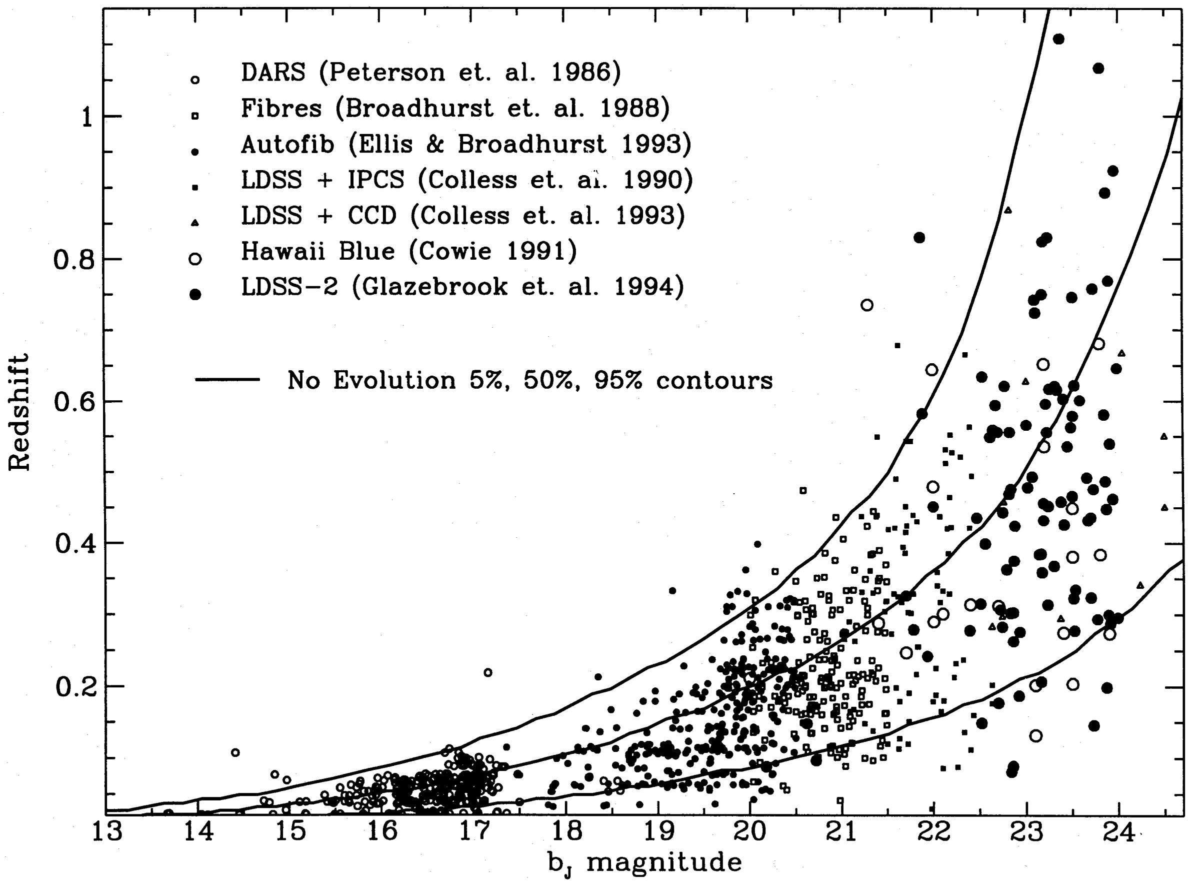

Figure 2. The magnitude–redshift distribution of the new data (total galaxy sample) compared to earlier work. The three solid lines show the contours below which lie 5, 50 and 95 per cent of the galaxies in the no-evolution model described in Section 4.3.1.

strong emission lines (e.g., Mg II, C III, C IV) in the UV should be easier to identify than galaxies.

QSO number–magnitude counts at bright magnitudes ($B<20$) (summarized by Hartwick & Schade 1990) are well fitted by a power law with slope 0.86. Extrapolated to $B=23.2$, this would predict 26 000 deg^{-2} mag^{-1}, which is far in excess of our limits, even allowing for the uncertainties. In contrast, our new survey, as that of Colless et al. (1991), supports the turnover in QSO counts defined by Koo, Kron & Cudworth (1986) and Boyle, Shanks & Peterson (1988) at $B=20$. While our formal errors are somewhat larger than those of the survey of compact objects by Colless et al., due to their larger sample, our independent result confirms their measurement in a fainter sample with no compactness criterion. Extrapolation of the flatter slope beyond $B=20$ predicts only 80 deg^{-2} mag^{-1} at $B=23.2$. While consistent with our numbers, there is the first indication of a somewhat larger number of QSOs than that found from UVX techniques alone (cf. Hawkins & Véron 1993).

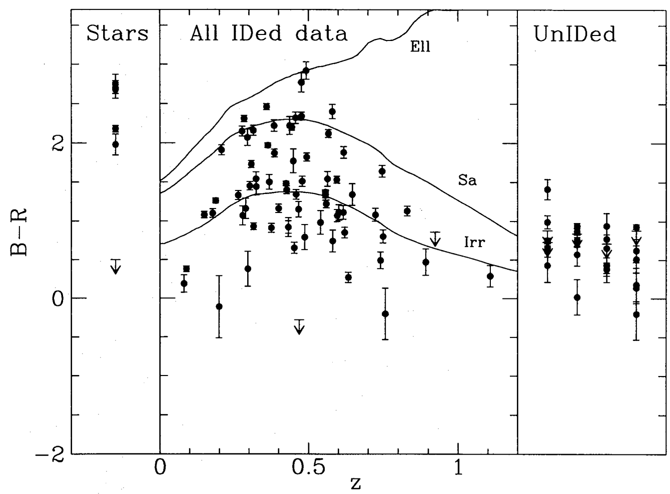

Figure 3. Optical colours as a function of redshift for the $B<B_{70\%}$ galaxy sample, together with those of stars and unidentified objects to the left and right. Arrows represent 3σ upper limits when $R>24$. Loci of some K-corrected non-evolving spectral types are shown.

4.2 Faint galaxy colours

Of the 111 objects in the $B<B_{70\%}$ sample, 108 have R data, and 100 have reliable $B-R$ colours to a limit of $R=24$. Fig. 3 shows the colour–redshift relation. On the left of the main plot we plot the colours of the stars, and on the right we plot those of the unidentified objects (although we do not mean to suggest that they are high-redshift objects). We also plot no-evolution loci for standard Hubble types; although we do see early-type galaxies, it is immediately obvious that their populations extend considerably more into the blue region than the templates, and that many have flat-spectrum colours ($B-R=0.2$). The number of galaxies in the $22.5<B<24$ sample is a factor of $(2-4)\times$ the no-evolution prediction, and the bulk of this blue excess is clearly identified as galaxies with $0.2 < z < 0.7$.

It is also clear that the unidentified objects in the $B < B_{70\%}$ sample are, on average, bluer than the identified sample and occupy a relatively narrow range in colour. For the purpose of constraining any evolutionary tail, it is important to determine the true redshift distribution of the unidentified population. We consider three possibilities.

(i) They could be very low-redshift ($z < 0.2$), low-luminosity systems. Although they have the appropriate colours, such objects would normally show spectra typical of H II regions, with strong emission lines of [O II], Hβ, [O III] and Hα. In our spectral window these should be the *easiest* objects to identify – not the hardest. The only possibility would be that they represented a class of object whose star formation had just ceased. However, in that case we would also expect to see many red systems with $z < 0.2$, so we conclude that this explanation is most unlikely.

(ii) They could have the same redshift distribution as the data ($0 < z < 1$). In this respect, it is curious that their redshifts were not determined. Fig. 4 demonstrates a strong correlation between the [O II] equivalent width and $B-R$ colour in our sample. This is probably not a selection effect arising from the absence of identified weak [O II] systems, since low-redshift samples (e.g. Kennicut 1992) also show the correlation. However, we cannot firmly rule out this possibility, and note that Colless et al. (1993) showed that the bluest systems in the unidentified LDSS-1 sample had $0 < z < 1$.

(iii) The final possibility is that the unidentified objects are at high redshifts, $z > 1$, and that the reason they remain unidentified is because [O II] is redshifted out of the spectral window leaving only weak absorption features (Mg II, Mg I) which are difficult to identify at low S/N ratios. Considering the earlier work of Colless et al. (1993), we do not believe this likely as the sole explanation since they found no such examples.

None of these hypotheses is convincing as a sole explanation; we expect that the most likely answer is a combination

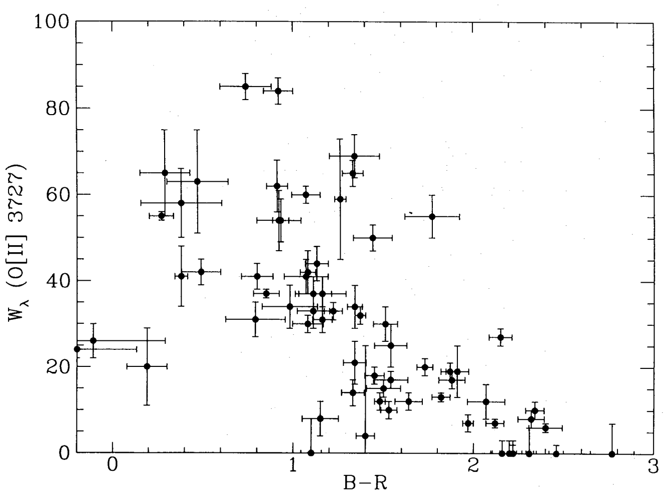

Figure 4. The [O II] 3727-Å emission line equivalent width versus optical colour. Points with $W_\lambda = 0$ are where the object has a redshift but no [O II] – in this case the error bar represents the upper limit.

of (ii) and (iii), as Colless et al. (1993) found some blue weak-lined [O II] systems at $z < 1$, and even in a no-evolution model we expect a number of galaxies at $B = 24$ to lie at $z > 1$ (see Section 4.3). When testing against models of luminosity evolution, as we will do in Section 4.3, the most conservative assumption is to place all the unidentified galaxies at $z > 1$, which gives an upper limit on the proportion of these galaxies. As we will demonstrate, our sample is sufficiently large and complete that our conclusions are not significantly altered by the placement of these galaxies.

4.3 The redshift distribution

The redshift distribution of the 73 galaxies in our 73 per cent complete subsample is shown in Fig. 5, together with the predictions of no-evolution and various evolutionary models, defined according to the parameters discussed by BEG.

4.3.1 The adopted zero-redshift luminosity function

We use a more recent luminosity function than BEG, with the Schechter parameters (M^*, α) for early- and late-type galaxies taken from Loveday et al. (1992) and a morphological mix adjusted to match the distribution of types seen at $b_J < 16.7$ by Shanks et al. (1984). We note that Zucca, Pozzetti & Zamorant (1994) recently suggested that the Loveday et al. analysis is in error; on reanalysis Zucca et al. obtain Schechter parameters closer to the older values of Efstathiou, Ellis & Peterson (1988). Our analysis below has been duplicated using the Efstathiou et al. (M^*, α) parameters: the conclusions remain unchanged.

The absolute normalization of the zero-redshift luminosity function ϕ^* currently remains uncertain by a factor of 2. If this is set higher, then this is equivalent to normalizing the no-evolution number–magnitude curve at a fainter apparent magnitude, and it lowers the excess of faint blue galaxies to be explained. Loveday et al. find a value of $\phi^* = 0.015\ h^3$ Mpc^{-3} from their luminosity function analysis based on bright $b_J < 17$ APM data. Metcalfe et al. (1991) argued that the normalization should be at $b_J = 19$ (equivalent to $\phi^* = 0.03\ h^3$ Mpc^{-3}), as the brighter data could be subject to local density fluctuations or calibration effects. These two values bracket the range of estimates in the literature; to be conservative, we adopt the higher value.

The model predictions are calculated, allowing for the variation of $B_{70\%}$ between fields. To normalize the models, we compute an effective area for each field, based on its magnitude limits and assuming a random sampling of the known number–magnitude counts. To allow for our field–field number fluctuations, we normalize to the number–magnitude counts of Jones et al. (1991), Lilly et al. (1991) and Metcalfe et al. (1991), which are much better determined over a larger area than in our survey, although our mean $22.5 < b_J < 24$ counts agrees well. Over the narrow range $22 < b_J < 25$ we find $\log\ (N/\mathrm{mag}^{-1}\ \mathrm{deg}^{-2}) = 2.62 + 0.43(b_J - 20)$ to be an excellent empirical fit to these data. Values for the effective areas thus calculated are given for each field in Table 2. For the more complete subsample, the total effective area is 14.2 arcmin^2.

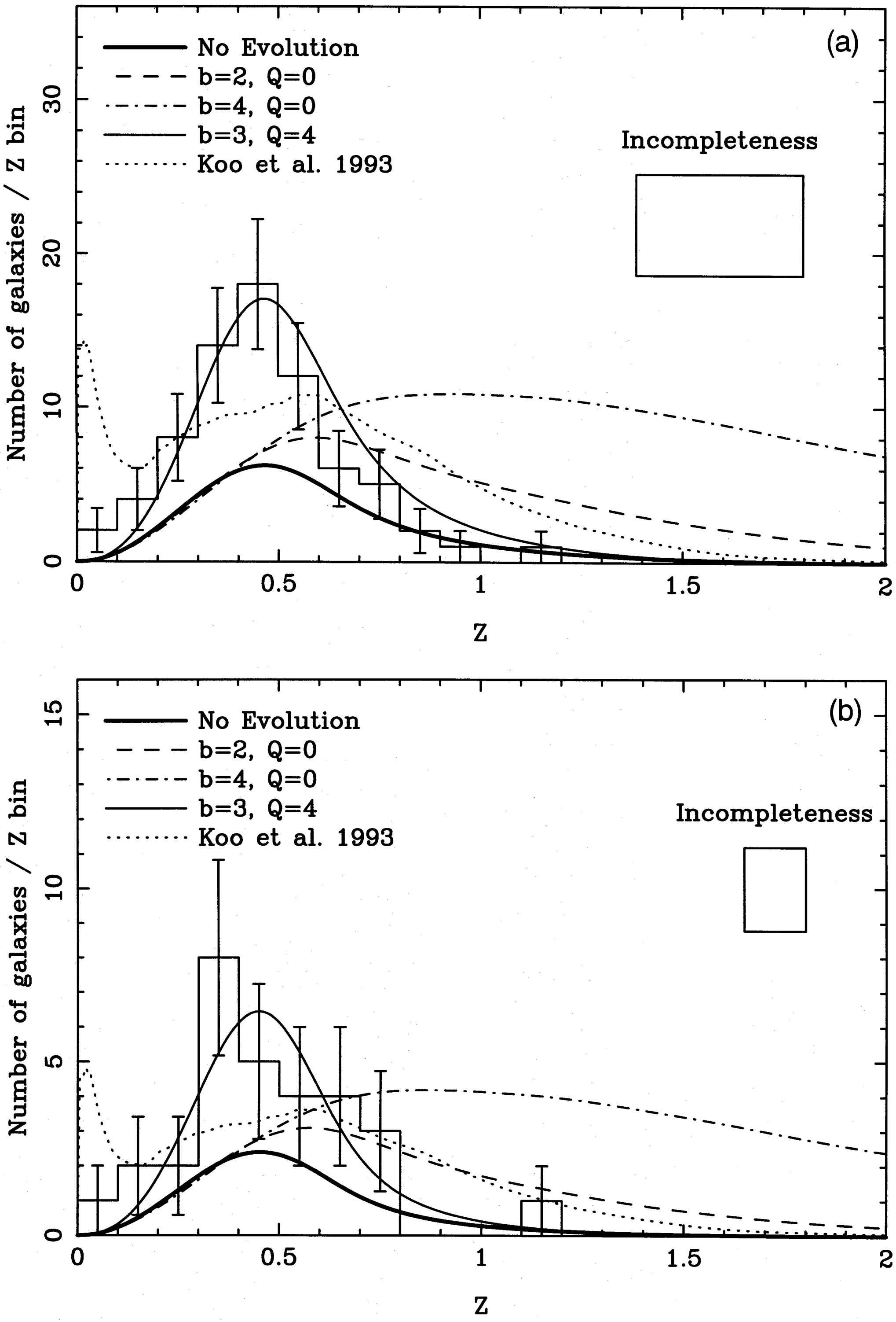

Figure 5. The redshift distribution of the new survey compared with the various galaxy evolution models described in the text: (a) the $B < B_{70\%}$ sample of 73 galaxies, and (b) the 89 per cent complete subsample of 30 galaxies.

4.3.2 *Correction for aperture effects*

One further issue is the aperture correction, i.e. the correction of the flux from the measured aperture to some notional 'total'. The conventional approach (e.g. Lilly 1993) is to use a small fixed aperture of 3–6 arcsec diameter and then correct to total by a fixed offset. Alternatively, a fixed isophote is used. Both of these will give redshift-dependent aperture effects; for example, our 4-arcsec aperture is 8 h^{-1} kpc at $z = 0.2$, and 17 h^{-1} kpc at $z = 1$ for $\Omega = 1$. A fixed isophote, in the observer's frame, gives still more severe effects due to the $(1+z)^4$ surface brightness dependence.

It would be possible to remeasure our magnitudes in metric apertures, now that the redshifts are known, but this would destroy the cleanness of our initial $22.5 < B < 24$ selection. Instead, we choose to correct our *models* to 4-

arcsec apertures; this has the additional advantage that all the cosmological dependence is kept in the model. Initially, for simplicity we used the growth law of Glazebrook et al. (1995, submitted), $L(<r) \propto r^{0.4}$, which is a good approximation to both standard exponential and de Vaucouleurs profiles outside the central few kpc. Indeed, Glazebrook et al. find this to be an excellent fit to their data. We correct to a standard aperture of 20 h^{-1} kpc, which gives a correction ranging from -0.37 mag at $z=0.2$ to -0.07 mag at $z=1$. In practice, the effect on the calculated redshift distribution for the range of models considered here turns out to be quite small, typically $\lesssim 0.5$ galaxies per redshift bin at the peak, because the correction is largest at low redshift where the volume is small. Thus a still more detailed treatment, such as using type-dependent exponential and de Vaucouleurs profiles according to the luminosity function weights, is unnecessary. The statistical results given below are unchanged by use of these aperture corrections.

4.3.3 *The evolutionary models*

BEG define the amount of luminosity evolution via the parameter b, which represents different exponential star formation time-scales, normalized so that the low-redshift evolution is $L \propto (1+bz)$. Curves for $b=0$ (no-evolution), $b=2$ and $b=4$ are plotted. To match the steep slope of the number counts, a $b=4$ luminosity evolution model was preferred by BEG. We also plot a BEG merger model ($b=3$, $Q=4$) which best fits the $n(z)$ where the Q parameter defines the rate of increase with look-back time in the number density. This model prediction is not too dissimilar to the no-evolution case when renormalized. Finally, we consider the recent model proposed by Koo et al. (1993), transformed from $dn/d\log z$ to dn/dz. (Note: strictly, Koo et al.'s model is for $23<B<24$ but, as this makes negligible difference to the data $n(z)$, we refrain from introducing another figure.) Koo et al.'s normalization is not specified in their paper, so we choose to scale their curve to match the total number of galaxies and unidentified objects in our sample.

The models are tested against the data in various ways, and the results are summarized in Table 4. First, we compare the overall shape of the distributions by means of a K–S test (P_{KS}). Secondly, we consider two less sensitive but more robust statistical tests, which allow us to make statistical statements *despite* the unidentified objects. The first of these considers the distribution of *median* redshifts. If we ignore the unidentified objects, the median redshift of our sample is $z_{MED}=0.46$. If we assume that all unidentified objects have $z>1$, then we obtain an upper limit to the median of $z_{MED}=0.56$. (Similarly, if they are all at $z\sim 0$, then $z_{MED}=0.36$.) Clearly, we can calculate a median redshift for the model distributions, but we need to assign a statistical significance to this. To do this, we generated 10^6 realizations of 100 redshifts (galaxies and unidentified objects), drawn randomly from the model distribution, and calculated the probability of observing $0.46<z_{MED}<0.56$, which we call P_{MED}.

Another interesting question is how does the fraction of high-redshift objects compare between the data and the various models? To quantify this, we measure $f_{0.7}$, the fraction of galaxies which have $z>0.7$. For the data, this is 0.12, rising to 0.38 if again we assume that all unidentified

Table 4. (a) Statistics of $n(z)$ models for $B<B_{70\%}$ sample. (b) Statistics of $n(z)$ models for 89 per cent complete subsample.

(a)	P_{KS}	z_{MED}	P_{MED}	$f_{0.7}$*	$P_{0.7}$*
Data	—	0.46	—	0.12	—
No Evolution	2×10^{-3}	0.53	0.88	0.26	1.00
$b=2$, $Q=0$	3×10^{-19}	0.83	$<10^{-6}$	0.61	3×10^{-6}
$b=4$, $Q=0$	9×10^{-37}	1.39	$<10^{-6}$	0.84	$<10^{-6}$
$b=3$, $Q=4$	2×10^{-2}	0.51	0.95	0.21	0.99
Koo *et al.* 1993	1×10^{-5}	0.56	0.50	0.36	0.73

(b)	P_{KS}	z_{MED}	P_{MED}	$f_{0.7}$*	$P_{0.7}$*
Data	—	0.46	—	0.13	—
No Evolution	0.45	0.49	0.17	0.19	0.62
$b=2$, $Q=0$	7×10^{-7}	0.76	8×10^{-5}	0.55	2×10^{-4}
$b=4$, $Q=0$	1×10^{-15}	1.31	$<10^{-6}$	0.82	$<10^{-6}$
$b=3$, $Q=4$	0.35	0.47	0.22	0.14	0.46
Koo *et al.* 1993	1×10^{-2}	0.56	5×10^{-2}	0.36	0.10

*See text for definitions.

objects are at $z>1$. We calculate $f_{0.7}$ for the models and the probability that $0.12<f_{0.7}<0.38$ ($P_{0.7}$), using the realizations which are tabulated in Table 4. Both P_{MED} and $P_{0.7}$ are sensitive to the global distribution over the whole $0<z<1$ range, and are thus insensitive to galaxy clustering on small scales. For the 89 per cent complete subsample we find a median redshift of 0.46 with limits (0.41, 0.48), and $f_{0.7}=0.13$ with limits (0.12, 0.24).

It can be seen from Fig. 5 that the $b=2$ and $b=4$ luminosity evolution models all predict too many high-redshift galaxies; this is confirmed statistically by the tests in Table 4. Note that the $b=2$ model is almost exactly equivalent to the mild luminosity evolution models advocated by Meltcalfe et al. (1991) and Koo & Kron (1992), and considered to be marginally consistent with the redshift distribution of Colless et al. (1990), given the incompleteness. Colless et al. (1993) reduced the incompleteness and found no $z>1$ galaxies; moreover, the bluest objects were at low redshift. Our extension to $B=24$ confirms this result, and reveals few $z>1$ galaxies.

Importantly, the data show a large excess of galaxies at $z\sim 0.4$ with respect to the no-evolution and luminosity evolution models. This is unaffected by the placement of the unidentified objects. Since we have used the highest possible local normalization of ϕ^*, this can only be an evolutionary effect. We are clearly seeing an increase in the space density of galaxies with $L\sim L_B^*$ ($z=0$). It is impossible for these simple luminosity evolution models to reproduce this, as they are only capable of adding extra galaxies above $z>0.7$.

In contrast, the merger model ($b=3$, $Q=4$) succeeds in matching the data both in shape and normalization, primarily because it involves little change in the bright end of the luminosity function while increasing the overall space density. No-evolution models which increase the number of galaxies at the faint end of the local luminosity function, such as that of Koo et al. examined here, produce a marked excess of $z<0.2$ galaxies *not* seen in our data, and do not match the excess of galaxies we *do* see at $z\sim 0.4$. The absence of low-redshift galaxies was already evident in Koo et al.'s own comparison, but was rather obscured by their use of an N–log z plot. This is one of the more significant conclusions arising from the new survey. The paucity of $z<0.2$ galaxies to $B=24$ severely constrains any possibility that the faint end of the local galaxy luminosity function has been severely underestimated, as Koo et al. conjectured.

5 CONCLUSIONS

The new redshift data presented here are a compelling piece of evidence ruling out simple luminosity evolution as the sole cause of the excess seen in the faint counts. Not only does the lack of high-redshift galaxies in a $B<24$ sample provide an even more severe limit than in brighter surveys, but the number of galaxies at *low* redshift ($z \sim 0.4$) clearly exceeds the predictions of luminosity evolution models for any reasonable value of the local normalization. Simple models of luminosity evolution cannot rectify this – we rule out any evolution in the bright end of the luminosity function. Importantly, there is also little scope for hypotheses which attempt to explain the faint count excess by modifying the zero-redshift luminosity function at the faint end, such as proposed by Koo et al. (1993) – LDSS-2 data have identified a *lower* envelope in the B–z diagram, which indicates that there is no such population. Moreover, such models cannot produce the *observed* excess seen at $z \sim 0.4$. Rather, evolution in the space density of blue galaxies with $L \sim L_B^*$ $(z=0)$ must occur, whatever the underlying mechanism. This could be explained by direct density evolution of galaxies of all luminosities, or differential luminosity evolution of only the lower luminosity galaxies up to $L \sim L_B^*$ $(z=0)$. Thus the conclusion that the total space density of luminous blue galaxies has changed since $z \sim 0.5$–1 becomes unavoidable.

ACKNOWLEDGMENTS

We especially thank the LDSS-2 team (Mike Breare, Keith Taylor, Dave Gellatly, Graham Shaw, John Webster and Sue Worswick) for the construction of an excellent instrument, and for providing support during the commissioning period. Further encouragement from Alex Boksenberg is gratefully acknowledged. The observations were carried out at the William Herschel Telescope, operated by the Royal Greenwich Observatory in the Spanish Observatorio del Roque de Los Muchachos of the Instituto de Astrofísica de Canarias. We thank Ian Smail for supplying the software for correcting the TAURUS images, and John Peacock, Chris Collins and Lance Miller for allowing the use of their photometric data. The data reduction was carried out using Starlink, which is funded by the PPARC. KGB, RSE and NRT acknowledge financial support by the PPARC.

REFERENCES

Allington-Smith J. R. et al., 1994, PASP, 106, 983
Babul A., Rees M. J., 1992, MNRAS, 255, 346
Boyle B. J., Shanks T., Peterson B. A., 1988, MNRAS, 235, 935
Broadhurst T. J., Ellis R. S., Shanks T., 1988, MNRAS, 235, 827
Broadhurst T. J., Ellis R. S., Glazebrook K., 1992, Nat, 355, 55 (BEG)
Colless M. M., Ellis R. S., Taylor K., Hook R. N., 1990, MNRAS, 244, 408
Colless M. M., Ellis R. S., Taylor K., Shaw G., 1991, MNRAS, 253, 686
Colless M. M., Ellis R. S., Broadhurst T. J., Taylor K., Peterson B. A., 1993, MNRAS, 261, 19
Cowie L. L., 1991, in Shanks T., Banday A. J., Ellis R. S., Frenk C. S., Wolfendale A. W., eds, Observational Tests of Cosmological Inflation. Kluwer, Dordrecht, p. 257
Cowie L. L., Songaila A., Hu E. M., 1991, Nat, 354, 460
Efstathiou G., Ellis R. S., Peterson B. A., 1988, MNRAS, 232, 431
Gehrels N., 1986, ApJ, 303, 336
Glazebrook K., Peacock J. A., Collins C. A., Miller L., 1994, MNRAS, 266, 65
Glazebrook K., Peacock J. A., Miller L., Collins C. A., 1995, MNRAS, submitted
Hartwick F. D. A., Schade D., 1990, ARA&A, 28, 437
Hawkins M. R. S., Véron P., 1993, MNRAS, 260, 202
Heydon-Dumbleton N. H., Collins C. A., MacGillivray H. T., 1989, MNRAS, 238, 379
Jones L. R., Fong R., Shanks T., Ellis R. S., Peterson B. A., 1991, MNRAS, 249, 481
Kennicut R. C., 1992, ApJ, 388, 310
Koo D. C., Kron R. G., 1992, ARA&A, 30, 613
Koo D. C., Kron R. G., Cudworth K. M., 1986, PASP, 98, 397
Koo D. C., Gronwall C., Bruzual G. A., 1993, ApJ, 415, L21
Lilly S. J., 1993, ApJ, 411, 501
Lilly S. J., Cowie L. L., Gardner J. P., 1991, ApJ, 369, 79
Loveday J., Peterson B. A., Efstathiou G., Maddox S. J., 1992, ApJ, 390, 338
Maddox S. J., Sutherland W. J., Efstathiou G., Loveday J., Peterson B. A., 1990, MNRAS, 247, 1P
Metcalfe N., Shanks T., Fong R., Jones L. R., 1991, MNRAS, 249, 498
Peterson B. A., Ellis R. S., Shanks T., Bean A. J., Fong R., Efstathiou G., Zou Z.-L., 1986, MNRAS, 221, 233
Rocca-Volmerange B., Guiderdoni B., 1990, MNRAS, 247, 166
Shanks T. S., Stevenson P. R., Fong R., MacGillivray H. T., 1984, MNRAS, 206, 767
Smail I., 1993, PhD thesis, Univ. Durham, England
Steidel C. C., Sargent W. L. W., 1992, ApJS, 80, 1
Thompson D. J., Djorgovski S., 1991, ApJ, 371, L55
Tresse L., Hammer F., Le Fèvre O., Proust D., 1993, A&A, 277, 53
Tyson J. A., 1988, AJ, 96, 1
Wynn C. G., Worswick S. P., 1988, Observatory, 108, 161
Zucca E., Pozzetti L., Zamorant G., 1994, MNRAS, 269, 953